Shear Strength of Wood Linear Friction Welded Joints: Experimental Study and Numerical Analysis

Liang Zhao [a], Hui Jin,[a,*] and Jie Wang [b]

Wood linear friction welding can be regarded as an environment-friendly and efficient wood connection technology. In this study, the welding depth, instead of welding time, was selected to control the whole welding process. The combination of welding amplitude of 1.7 mm, welding depth of 0.8 mm and welding pressure of 8 MPa was shown to be optimal by orthogonal experiments. Then the single factor tests were carried out to study the influence of welding amplitude, welding depth, and welding pressure on the shear strength of the welded joints. Finally, the effect of joint form and lap length on shear strength of welded joints was simulated and predicted with Cohesive Zone Models (CZM). It was found that the double lap joint had the greatest maximum shear strength compared with other three kinds of joints and shear strength of double lap joints would be enhanced with the increase of lap length almost linearly from 5 to 25 mm.

DOI: 10.15376/biores.20.4.10665-10684

Keywords: Wood friction welding; Welding depth; Welding amplitude; Welding pressure; Shear strength; CZM models

Contact information: a: Jiangsu Key Laboratory of Engineering Mechanics, School of Civil Engineering, Southeast University, Nanjing, 211189, China; b: Bureau of Housing and Urban-Rural Development of Jiangxia District, Wuhan, 430200, China; ** Corresponding author: jinhui@seu.edu.cn*

INTRODUCTION

Thermoplastic friction welding techniques, which are widely used in the plastic and car industries, can be applied to joining wood. Essentially, this is done by melting a thermoplastic polymer between the two wood surfaces to be joined (Gfeller *et al.* 2003). Without any adhesives, wood friction welding can give strength values comparable to those obtained with adhesive bonded joints (Pizzi *et al.* 2003). The time to complete a bond is less than 1 min, and no preparation of the welded surfaces is required (Stamm *et al.* 2005a), which leads to higher production efficiencies. Linear vibration welding is commonly used for laminated veneer lumber, glulam beams, and parquets (Leban *et al.* 2005).

To form wall, ceiling, or furniture elements with linear friction welding, the shear strength of welded joints has been tested. A shear strength of 2.0 MPa is sufficient for some applications such as the lamination of wooden slabs (Stamm *et al.* 2005a). The influencing parameters of strength are the machine settings (welding pressure, frequency, and amplitude of the movement) and the parameters of the material (species of wood, orientation of the annual rings, humidity, density and size) (Stamm *et al.* 2005b). Wood grain orientation differences in the two surfaces to be bonded yield bondlines of different strengths in linear wood welding (Omrani *et al.* 2009). The initial joint strength can be improved by welding shaped samples with an inclination of 45° (Hahn *et al.* 2015). Heat and chemical treatments also affect the shear strength of welded specimens, and the influence varies with the species of wood and species of treatments (Boonstra *et al.* 2006;

Zigon *et al.* 2015; Sun *et al.* 2019; Vaziri *et al.* 2020; Zor and Can 2021). Linear friction welding has been tested in untreated birch and beech (Boonstra *et al.* 2006), Scots pine (Vaziri *et al.* 2012), bamboo (Hu and Pizzi 2013; Zhang *et al.* 2014; Zhang *et al.* 2015), Brazilian *Eucalyptus benthamii* (Martins *et al.* 2013), Australian hardwood (Belleville *et al.* 2017), and crosswise arranged timber boards (Vallee *et al.* 2017).

For the machine settings, because of the differences in materials and interaction among welding parameters, a unified optimization law would not be formed easily. Delmotte *et al.* (2009) found that compared with the welding frequency of 100 Hz, 150 Hz resulted in an increase in crosslinking of the system. The effects involved crosslinking either of the lignin with itself or of the lignin with other wood constituents, contributing to the increased strength of the joint, which has been verified by Martins *et al.* (2013). However, Pizzi (2006) suggested that a welding frequency of 100 Hz, a 3-mm vibrational amplitude and a welding pressure of 2 to 2.3 MPa would give the best results of tensile strength. Compared with welding process parameters such as welding pressure, frequency and amplitude of the movement, welding time has been considered as a parameter to control the process. In a practical approach, an excessively long welding time (*i.e.*, longer than 2.5 s for welded beech and 8 s for welded spruce) would not provide an improvement in the mechanical properties but a further degradation of the wood components (Pena *et al.* 2016). This is because a minimal energy quantity has to be expended into the interphase to obtain satisfactory mechanical results and there is a maximal energy quantity which should not be exceeded to avoid a loss in bond strength (Ganne-Chedeville *et al.* 2008). But there are still some situations in which the welding time does not have a significant influence on the performance of the joint (Zhang *et al.* 2014). Cornuault and Carpentier 2020 suggested that the friction coefficient is a relevant tool in order to control the process in the goal of optimizing the mechanical strength of the welded assembly. In that work the friction coefficient was calculated from an energetic point and integrated throughout a single back-and-forth motion, during which the pin displacement, the friction force (F_T), and normal force (F_N) needed to be respectively measured thanks to a non-contact laser sensor, a piezoelectric sensor, and a gauge strain sensor. Undoubtedly, this process requires the cooperation of different kinds of sensors, and it is difficult to achieve a real-time control of the welding process. Consequently, in the present work the welded depth was selected as the parameter to control the welding process, which has been applied to wood dowel welding (Zhu *et al.* 2017).

Due to the influence of the machine settings and the parameters of the material, the optimization of strength needs a number of specimens to be tested. The techniques for strength prediction are essential. Vallee *et al.* (2011) described one probabilistic method that was based on a Weibull distribution and estimated the corresponding statistical parameters using the least squares/rank regression method and gathered stresses using FEA. Due to inconsistent test data, isolated predictions are of lower accuracy, though good agreement was obtained in the general trend. The same probabilistic method was also used by Hahn *et al.* (2012) to predict strength of linear welded double lap joints composed of timber, but the comparison between experimental and numerical result showed a significant discrepancy, herein 27% on average.

In recent years, cohesive zone models (CZM) have been used for the strength prediction, as an add-in to finite element (FE) analyses that allows simulation of damage growth (Campilho *et al.* 2013). In terms of wood material, CZM have been used to study fracture or damage characterization of wood (de Moura *et al.* 2006, 2010, 2018; Oliveira *et al.* 2007; Silva *et al.* 2007; de Moura and Dourado, 2018; Dourado *et al.* 2018, 2019;

Majano-Majano *et al.* 2019; Xavier *et al.* 2014a, b), medium density fiberboard (Matsumoto and Nairn 2009), wood-plastic composites (Alavi *et al.* 2015), glulam (Danielsson and Gustafsson 2014; Pavkovic *et al.* 2014), and cross-laminated timber (CLT) (Saavedra Flores *et al.* 2016). For wood joints, quasi-static behavior of steel-wood doweled joint (Caldeira *et al.* 2014), geometrical optimization of timber beech finger-joint (Tran *et al.* 2014a), bending behavior of beam-to-beam connection (Gecys *et al.* 2015) and CFRP-strengthened wood finger-joint (Khelifa *et al.* 2016), load-bearing capacity of multiple-tenon connection (Claus and Seim 2018), tensile performance of bolted glulam joints (Zhang *et al.* 2018), form optimization of timber-to-timber joints with self-tapping screws (Bedon and Fragiacomo 2019), and mechanical characterization of timber-to-timber composite (TTC) joints with self-tapping screws (Bedon *et al.* 2020) have been investigated with CZM. So, in this study, shear strength of wood linear friction welded joints with different forms and lap lengths was predicted with CZM after the determination and validation of model parameters in accordance with the experimental results.

EXPERIMENT

Raw Material

The friction welding material was beech (*Fagus sylvatica*). The density of the dried samples averaged 0.75 g/cm^3, which was measured after 24 h of drying in an oven at 103 ℃. The climate conditions (20 ℃ and 65% relative air humidity) were maintained until testing. The samples were welded in the longitudinal wood grain direction.

Grouping Scheme

To study the influence of welding pressure, welding amplitude (half of the distance between two endpoints during the welding process), and welding depth on shear strength, it is necessary to determine the optimal combination of three parameters in each group of specimens. A three factor mixed level orthogonal table L8 ($4^1 \times 2^4$) was selected. The specific level of each factor and the parameter list is shown in Table 1. The blank column in Table 1 represents the interactions of factors, which were not considered. Four levels of welding pressure (5, 6, 7, and 8 MPa), two levels of welding amplitude (1.5 and 1.7 mm), and two levels of welding depth (0.8 and 1.0 mm) were set. The determination of welding parameter values referred to presented studies (Stamm *et al.* 2005).

Table 1. Parameter List of Mixed Level Orthogonal Table L_8 ($4^1 \times 2^4$)

Group Number	Welding Pressure (MPa)		Welding Amplitude (mm)		Welding Depth (mm)		Empty Column	Empty Column
	Level Number	Value	Level Number	Value	Level Number	Value		
1	1	5	1	1.5	1	0.8	1	1
2	1	5	2	1.7	2	1	2	2
3	2	6	1	1.5	1	0.8	2	2
4	2	6	2	1.7	2	1	1	1
5	3	7	1	1.5	2	1	1	2
6	3	7	2	1.7	1	0.8	2	1
7	4	8	1	1.5	2	1	2	1
8	4	8	2	1.7	1	0.8	1	2

Testing Method

Welding process

The FW-951 vibration friction welding machine produced by Suzhou Keber Precision Machinery Co., Ltd. was used for wood friction welding. The welding frequency was 210 to 240 Hz, and the holding time was 30 s. Other welding parameters, such as welding depth, welding amplitude and welding pressure, were set through the controlling panel.

Fig. 1. Friction welding machine

Strength measurement

According to GB/T 50708-2012 technical specification for Glulam structures, the tensile shear test of wood friction welded joints was carried out. The wood joints used for tensile shear test were welded by two pieces of wood with the same size. Their size met the requirements of length L of 150 ± 5mm, width b of 20.0 ± 0.1mm and thickness t of 5.0 ± 0.1mm. A flat bottom notch with width of 2.0 ± 0.5 mm was made so that the overlapping length L_1 was 10.0 ± 0.1mm. The size of welded joints and the size of tensile shear specimens are shown in Fig. 2.

(a) Size of Welded Joints **(b)** Size of Tensile Shear Specimens

Fig. 2. Size of welded joints and size of tensile shear specimens

The tensile and shear tests were carried out on an INSTRON3367 double column bench type electronic testing machine with maximum force measuring capacity of 30 kN, accuracy of 0.5%, controllable displacement loading rate of 0.005 to 500 mm/min, and displacement control resolution of 0.054 μm. The loading process is shown in Fig. 3.

Fig. 3. Experimental loading process

The tensile shear strength of the welded specimen was calculated as follows,

$$\tau = \frac{P_{\mathrm{Max}}}{A} \quad (1)$$

where τ is the shear stress (N/mm^2), P_{Max} is the maximum failure load (N) when the specimen is damaged, and A is the welding surface area (mm^2), which was 20 mm × 10 mm = 200 mm^2.

RESULTS AND DISCUSSION

The tensile shear strength results of each group were the average strength of three identical specimens. The shear strength results of each welded joint of each group in the mixed orthogonal test are shown in Table 2. The highest tensile shear strength was obtained with the welding pressure of 8 MPa, the welding amplitude of 1.7 mm, and the welding depth of 0.8 mm.

Table 2. Tensile Shear Strength of Welded Joints in the Mixed Orthogonal Test

Group Number	Tensile Shear Strength (MPa)			Average Tensile Shear Strength (MPa)
	Specimen-3-1	Specimen-3-2	Specimen-3-3	
1	2.43	2.02	2.52	2.32
2	0.65	0.55	0.40	0.53
3	6.63	6.43	6.89	6.65
4	1.02	0.88	0.89	0.93
5	3.74	3.84	3.46	3.68
6	3.90	4.33	3.92	4.05
7	4.05	5.00	4.68	4.58
8	7.03	7.92	8.24	7.73

The mixed orthogonal test is beneficial for the selection and optimization of process parameters, but the method cannot determine the influence of parameter disturbance on the shear strength of welded joints. Therefore, on the basis of mixed orthogonal test, three groups of single variable tests were designed with reference to the optimal level of each parameter (8 MPa welding pressure, 1.7 mm welding amplitude, 0.8 mm welding depth). Through mechanical tests, the shear strength of welded joints was explored when welding pressure, welding amplitude and welding depth changed. The welding parameters of four groups of tests are shown in Table 3.

Table 3. Single Variable Test Parameters

Group Number	Welding Pressure (MPa)	Welding Amplitude (mm)	Welding Depth (mm)
A	4/6/8/10/12	1.7	0.8
B	8	1.4/1.5/1.6/1.7/1.8	0.8
C	8	1.7	0.4/0.6/0.8/1.0/1.2

Effect of Welding Pressure on Shear Strength

When the welding amplitude was 1.7 mm and the welding depth was 0.8 mm, the shear strength of the welded joints with different welding pressure is shown in Table 4. After welding, the molten material spilled from each group of welded joints with different welding pressure is shown in Fig. 4.

Table 4. Shear Strength of Welded Joints with Different Welding Pressure

Group Number	. Welding Pressure (MPa)	Tensile Shear Strength (MPa)			Average Tensile Shear Strength(MPa)
		Specimen-1	Specimen-2	Specimen-3	
A-1	4	1.00	0.68	0.57	0.75
A-2	6	1.00	1.10	0.90	1.00
A-3	8	2.15	1.70	3.60	2.49
A-4	10	2.75	3.62	4.10	3.49
A-5	12	6.10	4.35	5.60	5.35

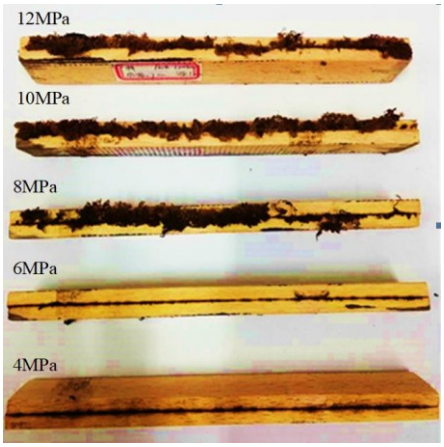

Fig. 4. Molten material of welded joints with different welding pressure

The shear strength increased with the increase of welding pressure. In the process of wood friction welding, the welding pressure affects the friction of the welding interface, and has an influence on the restructuring of molten cell structure in the later stage of welding. Specifically, the application of welding pressure can promote the recombination of molten fiber and intercellular material, make the welding layer material denser, and improve the welding strength. At the same time, the pressure would cause welding layer material to be squeezed out of the interface, and consequently reduce the effective fusion interface material, and weaken the bonding strength. According to Fig. 4, compared with the welding specimens with 4 and 6 MPa welding pressure, the welding specimens with 8, 10, and 12 MPa welding pressure had more spilled wood fiber in the welding process. It can be inferred that the reason why the shear strength increased rapidly when the welding pressure was less than 8 MPa is that with the increase of welding pressure, the friction coefficient of the welding interface increases, and more heat is generated to promote the melting of the interface cells. As a result, the molten material formed a denser welding layer under the effect of pressure (Leban *et al.* 2004), which made the shear strength increase significantly, from 1.00 to 2.49 MPa. When the welding pressure was greater than 8 MPa, the shear strength increased slowly, because the overflow of wood fiber increased, and, as a result, the generation and overflow of effective bonding material retained in the welding layer reached a balance. In addition, excessive welding pressure would cause a sharp increase in the temperature of the welding interface, leading to interface burning and carbonization, thereby reducing the strength of the welding interface (Omrani *et al.* 2010).

Effect of Welding Amplitude on Shear Strength

When the welding pressure was 8 MPa and the welding depth was 0.8 mm, the shear strength of the welded joints with different welding amplitude is shown in Table 5. After welding, the molten material spilled from each group of welded joints under different welding amplitude is shown in Fig. 7.

Table 5. Shear Strength of Welded Joints with Different Welding Amplitude

Group Number	Welding Amplitude (mm)	Tensile Shear Strength (MPa)			Average Tensile Shear Strength (MPa)
		Specimen-1	Specimen-2	Specimen-3	
B-1	1.4	4.95	6.55	4.22	5.24
B-2	1.5	3.65	4.14	3.91	3.90
B-3	1.6	1.60	1.95	2.87	2.14
B-4	1.7	1.00	1.04	0.90	0.98
B-5	1.8	1.06	0.88	1.06	1.00

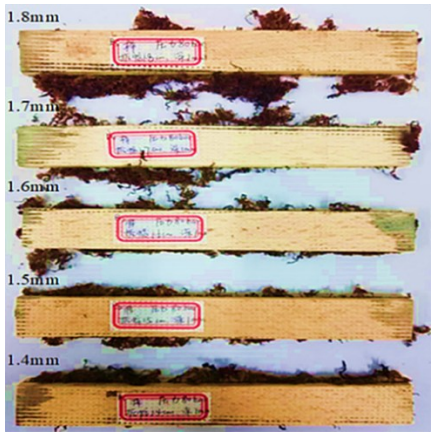

Fig. 5. Molten material of welded joints with different welding amplitude

Figure 7 shows that the shear strength of beech decreased with the increase of welding amplitude. When the welding amplitude was 1.5, 1.6, 1.7, and 1.8 mm, the shear strength decreased by 25.5%, 45.3%, 54.3%, and 2.6% compared with the previous welding amplitude. When the welding amplitude was 1.7 and 1.8 mm, the shear strength was only 0.975 and 1 MPa. With the increase of welding amplitude, the amount of wood fiber overflowing from the joint increased gradually. This was because the vibration speed of the welding equipment increased in order to meet the requirements of increased amplitude without changing the frequency. When the vibration speed was low, increasing the vibration speed would increase the interface temperature, which contributes to increasing the melting of the cell material. However, if the vibration speed is too high, interlaced fibers in the welding layer dislocate or fracture, which weakens the shear strength of joints.

Effect of Welding Depth on Shear Strength

When the welding pressure was 8 MPa and the welding amplitude was 1.7 mm, the shear strength of the welded joints with different welding depth is shown in Table 6. After welding, the molten material spilled from each group of welded joints under different welding depth is shown in Fig. 6.

Table 6. Shear Strength of Welded Joints with Different Welding Depth

Group Number	Welding Depth (mm)	Tensile Shear Strength (MPa)			Average Tensile Shear Strength (MPa)
		Specimen-1	Specimen-2	Specimen-3	
C-1	0.4	11.55	11.80	11.65	11.67
C-2	0.6	11.80	12.85	9.45	11.37
C-3	0.8	6.70	5.65	6.85	6.40
C-4	1.0	3.75	3.80	3.77	3.78
C-5	1.2	2.44	3.35	2.10	2.63

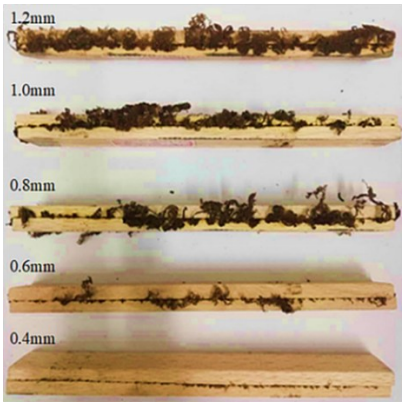

Fig. 6. Molten material of welded joints under different welding depth

The welding depth controlled by fw-951 linear friction welding machine refers to the relative displacement of two welding interfaces, that is, the extrusion degree between the two welding blocks, rather than the thickness of the welding layer. As shown in Table 6, with the increase of welding depth, the shear strength first decreased slowly, and then it decreased sharply. The difference of shear strength with welding depth of 0.4 and 0.6 mm was small. When the welding depth increased from 0.6 to 1.2 mm, the shear strength showed an obvious downward trend, from 11.37 to 2.62 MPa. At a greater welding depth, more fibers were spilled. When the welding depth is small, the appropriate increase of extrusion on the welding layer is conducive to the reorganization of the molten fiber in the welding layer, which improves the density of the welding layer. However, when the welding depth is more than 0.6 mm, increasing the depth would lead to excessive extrusion of the fibers in the welding layer, and eventually reduce the shear strength of joints.

Strength Prediction with CZM Model

After obtaining the optimal combination of welding depth, welding pressure and welding amplitude, the CZM model was applied to verify the effects of joint forms and lap lengths on the shear strength of wood linear friction welded joints.

Model Parameters Determination and Validation

According to the brittle failure characteristic of wood linear friction welded joints under tensile shear load, a bilinear CZM model was used to simulate the delamination and failure process of wood linear friction welded interface. The formulation is based on the constitutive relationship between stresses on the crack plane and the corresponding relative displacements (de Moura *et al.* 2006), which is according to Eq. 1. The method requires the local strengths (σ_i, i = I, II, III) and the critical strain energies release rates ($\emptyset_i^c$) as

inputted data parameters (Silva *et al.* 2007),

$$\sigma_i = \begin{cases} \frac{\sigma_i^{max}}{\delta_i^0}\delta_i \ (\delta_i \le \delta_i^0) \\ \sigma_i^{max}\frac{\delta_i^f - \delta_i}{\delta_i^f - \delta_i^0} \ (\delta_i > \delta_i^0) \end{cases} (i = \mathrm{I, II, III}) \quad (2)$$

where $\sigma_i (i = \mathrm{I, II, III})$ is stress of mode I, mode II, and mode III failure, and $\sigma_i^{max} (i = \mathrm{I, II, III})$ is maximum stress of mode I, mode II, and mode III failure, and the corresponding crack interface opening displacement is $\delta_i^0 (i = \mathrm{I, II, III})$. After reaching its maximum stress, the stress begins to decrease, and when it reaches zero, the cracking is completed, and the corresponding displacement is the final cracking displacement$\delta_i^f (i = \mathrm{I, II, III})$. The corresponding fracture energy $\emptyset_i^c (i = \mathrm{I, II, III})$ was calculated as follows,

$$\emptyset_i^c = \frac{1}{2}\sigma_i^{max}\delta_i^f (i = \mathrm{I, II, III}) \quad (3)$$

To determine the parameters of wood linear friction welding CZM model, three wood friction welded joints with welding pressure of 8 MPa, welding amplitude of 1.7 mm, and welding depth of 1 mm were selected. It was assumed that the three modes have the same maximum stress, crack interface opening displacement, and final cracking displacement. The elastic deformation of the friction welding layer was ignored; that is, the mode II crack opening displacement is the displacement of the joint under tensile-shear load. The CZM parameters of the three joints under the shear load are shown in Table 7.

Table 7. CZM Parameters of the Three Joints Under Shear Load

Group Number	τ_{max} (MPa)	δ_t^0 (mm)	δ_t^f (mm)	$\emptyset_t^c$ (mJ/mm^2)
C-4-1	3.75	0.470	0.473	0.887
C-4-2	3.80	0.497	0.502	0.954
C-4-3	3.77	0.475	0.482	0.909
Average	3.78	0.481	0.486	0.917

The average value of CZM parameters of three joints was used as the parameter input value of ABAQUS built-in bilinear CZM model. The secondary stress criterion was chosen as the damage initiation criterion; its formula is:

$$\left\{\frac{\langle\sigma_{\mathrm{I}}\rangle}{\sigma_{\mathrm{I}}^{\max}}\right\}^2 + \left\{\frac{\sigma_{\mathrm{II}}}{\sigma_{\mathrm{II}}^{\max}}\right\}^2 + \left\{\frac{\sigma_{\mathrm{III}}}{\sigma_{\mathrm{III}}^{\max}}\right\}^2 = 1 \quad (4)$$

where, $\sigma_{\mathrm{I}}^{\max}$,$\sigma_{\mathrm{II}}^{\max}$,$\sigma_{\mathrm{III}}^{\max}$ are maximum stress of mode I, mode II and mode III failure. The < > item is the McCauley bracket, indicating that the effect of normal stress and strain on damage is not considered when the cohesive element is under compression. In the calculation process, when the output value of the given initial damage criterion is greater than or equal to 1, the damage begins. In ABAQUS, the initial damage variable Quadscrt can be used to monitor the damage state of the interface element. In addition, the power exponent criterion was chosen as the damage evolution criterion; its representation is:

$$\left\{\frac{G_{\mathrm{I}}}{G_{\mathrm{I}}^{\mathrm{c}}}\right\}^{\alpha} + \left\{\frac{G_{\mathrm{II}}}{G_{\mathrm{II}}^{\mathrm{c}}}\right\}^{\alpha} + \left\{\frac{G_{\mathrm{III}}}{G_{\mathrm{III}}^{\mathrm{c}}}\right\}^{\alpha} = 1 \quad (5)$$

where, G_{I}, G_{II}, G_{III} are energy release rates of type I, type II and type III failure, and $G_{\mathrm{I}}^{\mathrm{c}}$, $G_{\mathrm{II}}^{\mathrm{c}}$, $G_{\mathrm{III}}^{\mathrm{c}}$ are critical energy release rates of mode I, mode II and mode III failure. The value of α was 2. When the energy release rate and the critical energy release rate of the

cohesive unit meet the relationship shown in Eq. 4, the cohesive unit would fail completely.

The model used in the numerical simulation has the same size as the joint used in the test, *i.e.*, two pieces of wood with the length L of 150 mm, width *b* of 20.0 mm and thickness *t* of 5.0 mm. The area of the welding interface under tensile shear load is 200 mm^2. The boundary conditions of model is that one end of the model is completely fixed, and the other end is applied with displacement load. Elastic properties of beech are shown in Table 8. The displacement-load curves of tested and numerically simulated welded joints are shown in Fig. 7.

The numerical simulation results of CZM model were found to match well with the test results of three joints in the rising stage of load displacement curve. The average maximum tangential load of three tested joints was 742 N, and the maximum tangential load obtained from the numerical simulation of CZM model was 716 N. The relative deviation between them was only 3.5%. Therefore, the CZM model with parameters on the basis of tests can well predict the strength of wood linear friction welded joints under shear load.

However, there were significant differences between the experimental and numerical stiffness after the maximum tangential loads were reached. This is because compared to the uniform and ideal interface model established in the numerical simulation process, there were areas of ineffective welding and uneven welding formed in the actual friction welding process. Therefore, after the welding layer reached its maximum tension and begins to break, the ineffective welding area would quickly detach and lose its load-bearing capacity.

Table 8. Elastic Properties of Beech (Tran *et al.* 2014b)

E_L (GPa)	E_R (GPa)	E_T (GPa)	υ_{RT}	υ_{LR}	υ_{TR}	G_{RT} (GPa)	G_{LR} (GPa)	G_{TL} (GPa)
14.788	1.848	1.087	0.67	0.39	0.38	0.366	1.260	0.971

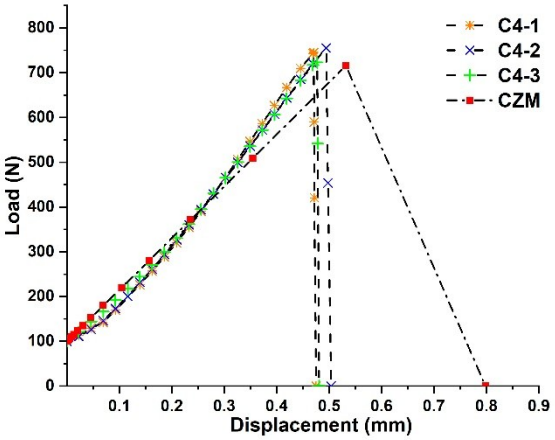

Fig. 7. Displacement-load curves of tested and simulated welded joints

Effect of Joint Form on Shear Strength

After the determination and validation of parameters, the failure behavior of four common kinds of joints including single lap joints, double lap joints, single cover butt joints, and double cover butt joints were analyzed with use of the CZM modal. The welding

area of four kinds of joints was 200 mm^2 with the width of 20mm, and their specific forms and sizes are shown in Fig. 8.

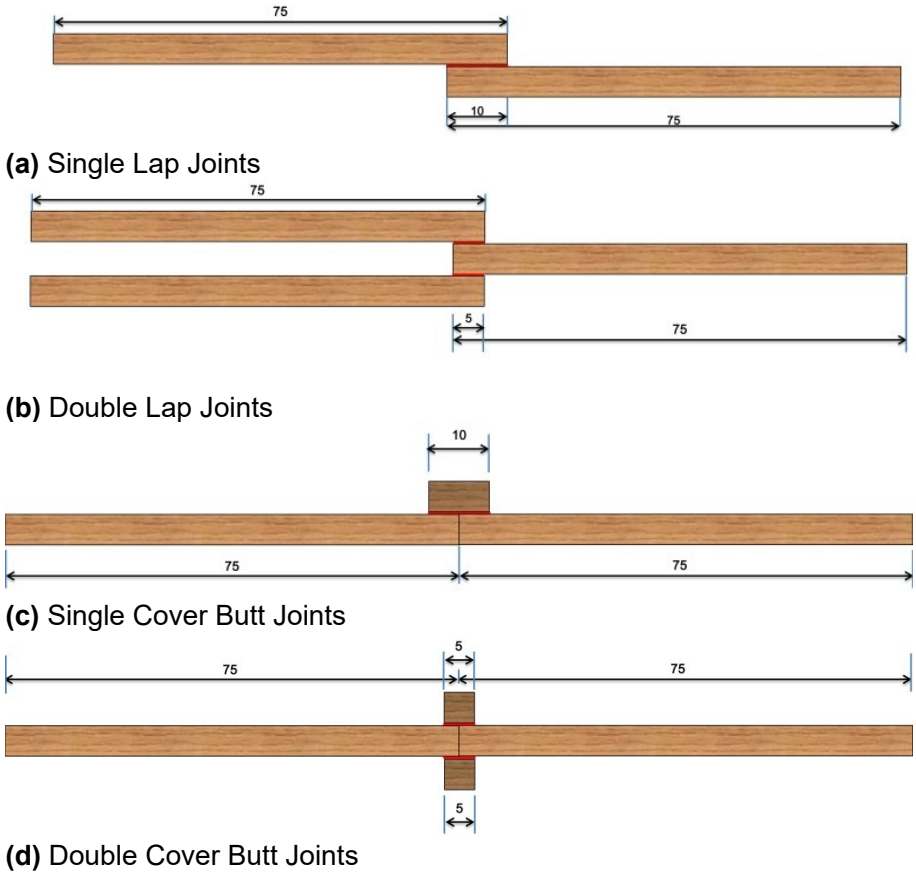

Fig. 8. Forms and sizes of joints

Maximum tangential loads, initial cracking displacements and final cracking displacements of four kinds of joints are shown in Table 9, and their displacement-load curves are shown in Fig. 9. The double lap joint had the greatest maximum tangential load compared with other three kinds of joints, which is due to the symmetry of the form and uniformly distributed stress. As shown in Fig. 10, which indicates the stress of cohesive elements when joints reach the maximum tangential load, the difference between the maximum and minimum stress of cohesive elements of the double lap joint was just 0.026 MPa, which was 0.05, 1.603, and 0.038 MPa less than the difference of the single lap joint, the single cover butt joint, and the double cover butt joint, respectively.

Table 9. Maximum Tangential Loads, Initial and Final Cracking Displacements of Joints with Different Joint Forms

Joint Form	Maximum Tangential Loads (N)	Initial Cracking Displacements (mm)	Final Cracking Displacements (mm)
Single Lap	687.9	0.665	0.997
Double Lap	729.8	0.551	0.562
Single Cover Butt	146.0	0.875	1.000
Double Cover Butt	616.9	0.874	1.312

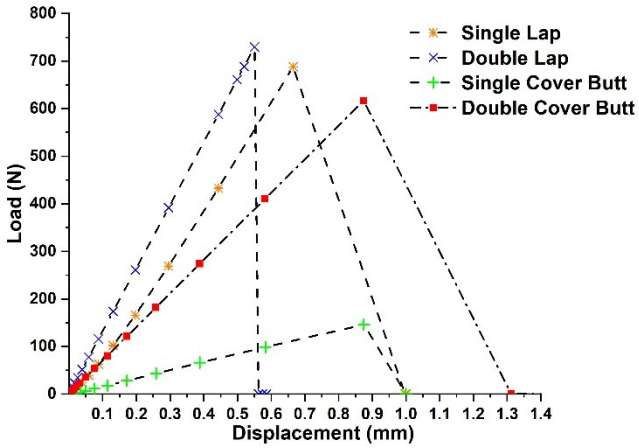

Fig. 9. Displacement-load curves of joints with different forms

The initial damage variables of cohesive elements of joints when they reach the maximum tangential load are shown in Fig. 11. For the double lap joint, the minimum value of QUADECRT was 0.970, which means that almost all the cohesive elements would start to fail after the maximum tangential load has been applied to the joint; that is, all the cohesive elements contributed to the bearing of loads. On the contrary, the minimum values of QUADECRT of the single lap joint, the single cover butt joint, and the double cover butt joint were just 0.853, 0.127, and 0.685, respectively. Only a fraction of elements were fully loaded during the loading process, which indicates the waste of bearing capacity of friction welding interfaces.

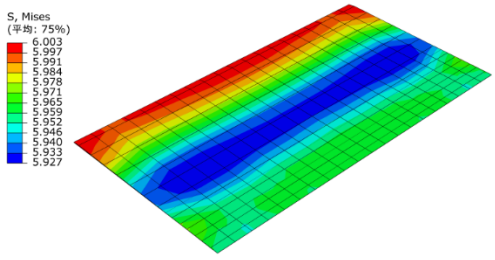

(a) Single Lap Joints

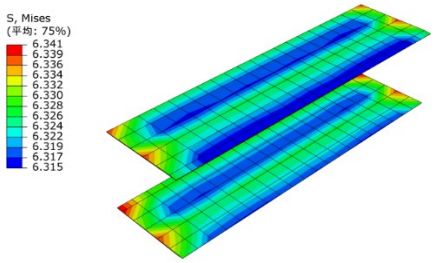

(b) Double Lap Joints

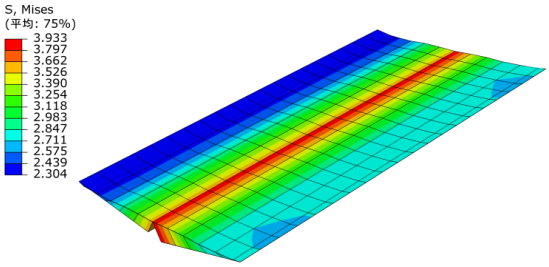

(c) Single Cover Butt Joints

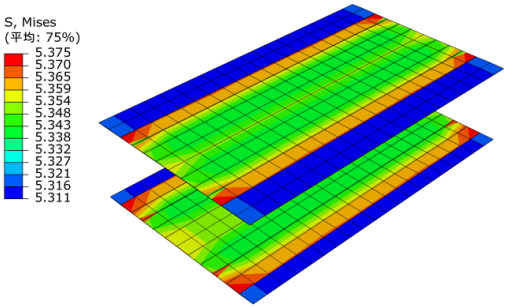

(d) Double Cover Butt Joints

Fig. 10. Stress of cohesive elements with the maximum tangential load

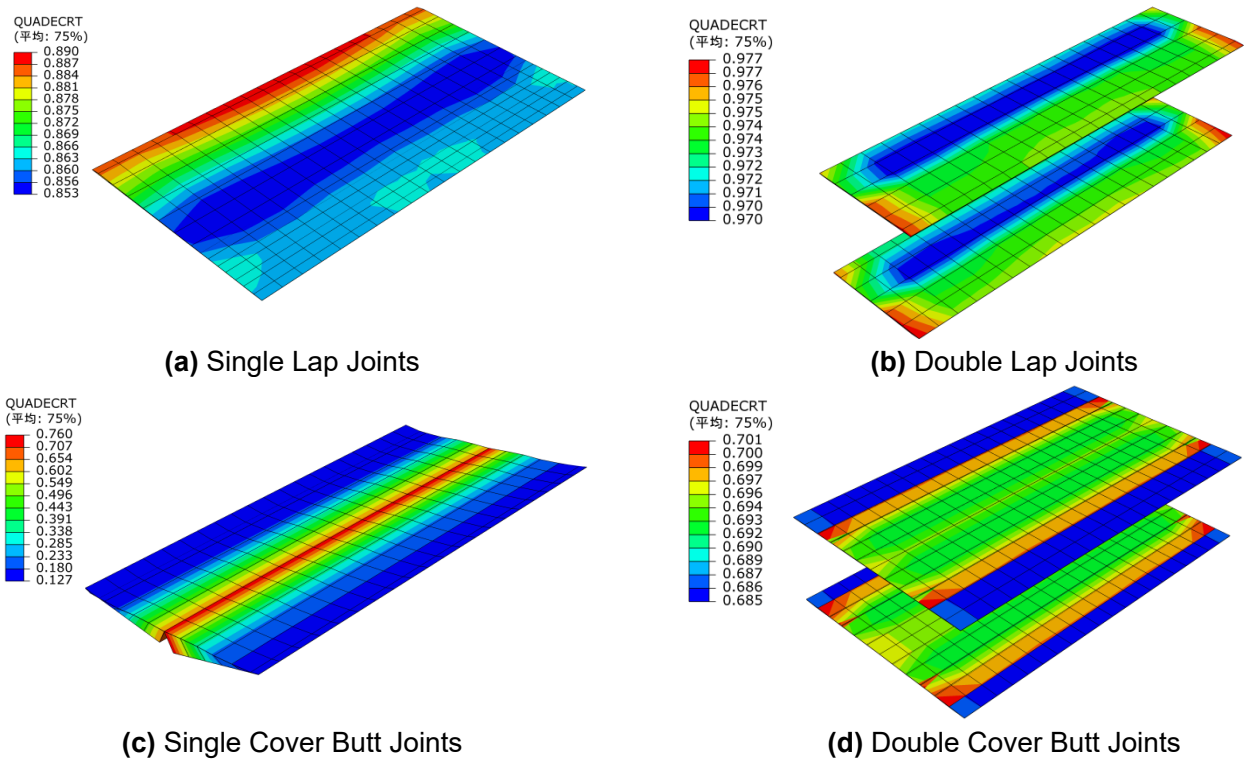

(a) Single Lap Joints **(b)** Double Lap Joints

(c) Single Cover Butt Joints **(d)** Double Cover Butt Joints

Fig. 11. Initial damage variables of cohesive elements with the maximum tangential load

Effect of Lap Length on Shear Strength

After the analysis of the effect of joint forms on the shear strength, the double lap joint was selected to evaluate the effect of lap length on shear strength of welded joints.

Table 10. Maximum Tangential Loads, Initial and Final Cracking Displacements of Joints with Different Lap Lengths

Lap Length(mm)	Maximum Tangential Loads (N)	Initial Cracking Displacements (mm)	Final Cracking Displacements (mm)
5	729.8	0.551	0.562
10	1229.4	0.517	0.776
15	1441.7	0.436	0.663
20	2771.5	0.663	1.005
25	3315.6	0.663	1.005

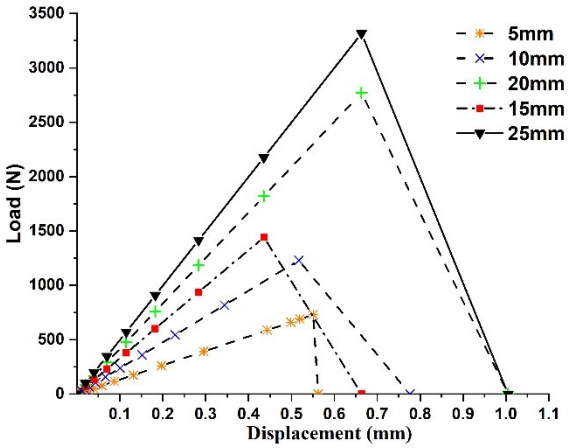

Fig. 12. Displacement-load curves of joints with different lap lengths

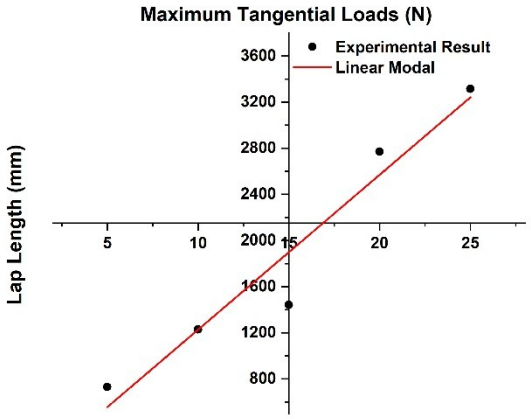

Fig. 13. Linear modal of maximum tangential loads with different lap lengths

The lengths of 5, 10, 15, 20, and 25 mm were set with the same width of 20 mm. Maximum tangential loads, initial cracking displacements, and final cracking displacements of joints with different lap lengths are shown in Table 10, and their displacement-load curves are shown in Fig. 12. For double lap joints, the increase of lap length would significantly improve the maximum tangential load and the final cracking displacement. As shown in Fig. 13, because the value of Pearson's R is 0.9698, the increase of maximum is almost linear with the overlap length, which is in consistent with the predicted result of the probabilistic method (Vallee *et al.* 2011).

CONCLUSIONS

1. Welding depth can be used to control the whole welding process precisely. For beech, the optimal combination of welding parameters was found to be a welding amplitude of 1.7 mm, welding depth of 0.8 mm, and welding pressure of 8 MPa. The shear strength is improved with the increase of welding pressure but the increase of welding

amplitude and welding depth would not enhance the shear strength of welded joints, which is mainly due to that more fibers would be spilled from welded interference during welding process.

2. Cohesive Zone Models (CZM) with parameters determined from tests can well predict the strength of wood linear friction welded joints under shear load. Double lap joints have the greatest maximum shear strength compared with single lap joints, single cover butt joints, and double cover butt joints. For double lap joints, shear strength would be improved with the increase of lap length almost linearly from 5 to 25 mm.

REFERENCES CITED

Alavi, F., Behravesh, A.H., and Mirzaei, M. (2015). "Mixed-mode cohesive zone modeling and damage prediction of irregular-shaped interfaces in wood-plastic composites," *Composite Interfaces* 22(7), 651-662. DOI: 10.1080/09276440.2015.1058671

Bedon, C., and Fragiacomo, M. (2019). "Numerical analysis of timber-to-timber joints and composite beams with inclined self-tapping screws," *Composite Structures* 207, 13-28. DOI: 10.1016/j.compstruct.2018.09.008

Bedon, C., Sciomenta, M., and Fragiacomo, M. (2020). "Mechanical characterization of timber-to-timber composite (TTC) joints with self-tapping screws in a standard push-out setup," *Applied Sciences-Basel* 10(18), article 6534. DOI: 10.3390/app10186534

Belleville, B., Amirou, S., Pizzi, A., and Ozarska, B. (2017). "Optimization of wood welding parameters for Australian hardwood species," *BioResources* 12(1), 1007-1014. DOI: 10.15376/biores.12.1.1007-1014

Boonstra, M., Pizzi, A., Ganne-Chedeville, C., Properzi, M., Leban, J. M., and Pichelin, F. (2006). "Vibration welding of heat-treated wood," *Journal of Adhesion Science and Technology* 20(4), 359-369. DOI: 10.1163/156856106776381758

Caldeira, T. V. P., Dourado, N., de Jesus, A. M. P., de Moura, M. F. S. F., and Morais, J. J. L. (2014). "Quasi-static behavior of moment-carrying steel-wood doweled joints," *Construction and Building Materials* 53, 439-447. DOI: 10.1016/j.conbuildmat.2013.11.078

Campilho, R. D. S. G., Banea, M. D., Neto, J. A. B. P., and da Silva, L. F. M. (2013). "Modelling adhesive joints with cohesive zone models: effect of the cohesive law shape of the adhesive layer," *International Journal of Adhesion and Adhesives* 44, 48-56. DOI: 10.1016/j.ijadhadh.2013.02.006

Claus, T., and Seim, W. (2018). "Development of the multiple tenon timber connection based on experimental studies and FE simulation," *Engineering Structures* 173, 331-339. DOI: 10.1016/j.engstruct.2018.06.102

Cornuault, P. H., and Carpentier, L. (2020). "Tribological mechanisms involved in friction wood welding," *Tribology International* 141, 11. DOI: 10.1016/j.triboint.2019.105963

Danielsson, H., and Gustafsson, P. J. (2014). "Fracture analysis of glued laminated timber beams with a hole using a 3D cohesive zone model," *Engineering Fracture Mechanics* 124, 182-195. DOI: 10.1016/j.engfracmech.2014.04.020

de Moura, M., Silva, M. A. L., de Morais, A. B., and Morais, J. J. L. (2006). "Equivalent crack based mode II fracture characterization of wood," *Engineering Fracture Mechanics* 73(8), 978-993. DOI: 10.1016/j.engfracmech.2006.01.004

de Moura, M. F. S. F., and Dourado, N. (2018). "Mode I fracture characterization of wood using the TDCB test," *Theoretical and Applied Fracture Mechanics* 94, 40-45. DOI: 10.1016/j.tafmec.2018.01.005

de Moura, M. F. S. F., Oliveira, J. M. Q., Morais, J. J. L., and Xavier, J. (2010). "Mixed-mode I/II wood fracture characterization using the mixed-mode bending test," *Engineering Fracture Mechanics* 77(1), 144-152. DOI: 10.1016/j.engfracmech.2009.09.014

de Moura, M. F. S. F., Silva, M. A. L., Morais, J. J. L., and Dourado, N. (2018). "Mode II fracture characterization of wood using the four-point end-notched flexure (4ENF) test," *Theoretical and Applied Fracture Mechanics* 98, 23-29. DOI: 10.1016/j.tafmec.2018.09.008

Delmotte, L., Mansouri, H. R., Omrani, P., and Pizzi, A. (2009). "Influence of wood welding frequency on wood constituents chemical modifications," *Journal of Adhesion Science and Technology* 23(9), 1271-1279. DOI: 10.1163/156856109X433991

Dourado, N., de Moura, M. F. S. F., and de Jesus, A. (2019). "Fatigue-fracture characterization of wood under mode I loading," *International Journal of Fatigue* 121, 265-271. DOI: 10.1016/j.ijfatigue.2018.12.012

Dourado, N., Silva, F. G. A., and de Moura, M. F. S. F. (2018). "Fracture behavior of wood-steel dowel joints under quasi-static loading," *Construction and Building Materials* 176, 14-23. DOI: 10.1016/j.conbuildmat.2018.04.230

Ganne-Chedeville, C., Properzi, M., Leban, J. M., Pizzi, A., and Pichelin, F. (2008). "Wood welding: Chemical and physical changes according to the welding time," *Journal of Adhesion Science and Technology* 22(7), 761-773. DOI: 10.1163/156856108X306939

Gecys, T., Daniunas, A., Bader, T.K., Wagner, L., and Eberhardsteiner, J. (2015). "3D finite element analysis and experimental investigations of a new type of timber beam-to-beam connection," *Engineering Structures* 86, 134-145. DOI: 10.1016/j.engstruct.2014.12.037

Gfeller, B., Zanetti, M., Properzi, M., Pizzi, A., Pichelin, F., Lehmann, M., and Delmotte, L. (2003). "Wood bonding by vibrational welding," *Journal of Adhesion Science and Technology* 17(11), 1573-1589. DOI: 10.1163/156856103769207419

Hahn, B., Stamm, B., and Weinand, Y. (2015). "Influence of surface shapes on the mechanical behaviour of friction welded wood bonds," *European Journal of Wood and Wood Products* 73(1), 29-34. DOI: 10.1007/s00107-014-0846-0

Hahn, B., Vallee, T., Stamm, B., and Weinand, Y. (2012). "Experimental investigations and probabilistic strength prediction of linear welded double lap joints composed of timber," *International Journal of Adhesion and Adhesives* 39, 42-48. DOI: 10.1016/j.ijadhadh.2012.06.004

Hu, J. B., and Pizzi, A. (2013). "Wood-bamboo-wood laminated composite lumber jointed by linear vibration-friction welding," *European Journal of Wood and Wood Products* 71(5), 683-686. DOI: 10.1007/s00107-013-0714-3

Khelifa, M., Celzard, A., Oudjene, M., and Ruelle, J. (2016). "Experimental and numerical analysis of CFRP-strengthened finger-jointed timber beams," *International Journal of Adhesion and Adhesives* 68, 283-297. DOI: 10.1016/j.ijadhadh.2016.04.007

Leban, J. M., Pizzi, A., Properzi, M., Pichelin, F., Gelhaye, P., and Rose, C. (2005). "Wood welding: A challenging alternative to conventional wood gluing,"

Scandinavian Journal of Forest Research 20(6), 534-538. DOI: 10.1080/02827580500432305

Leban, J. M., Pizzi, A., Wieland, S., Zanetti, M., Properzi, M., and Pichelin, F. (2004). "X-ray microdensitometry analysis of vibration-welded wood," *Journal of Adhesion Science and Technology* 18(6), 673-685. DOI: DOI: 10.1163/156856104839310

Majano-Majano, A., Jose Lara-Bocanegra, A., Xavier, J., and Morais, J. (2019). "Measuring the cohesive law in mode I loading of *Eucalyptus globulus*," *Materials* 12(1), article 23. DOI: 10.3390/ma12010023

Martins, S.A., Ganier, T., Pizzi, A., and Del Menezzi, C.H.S. (2013). "Parameter scanning for linear welding of Brazilian *Eucalyptus benthamii* wood," *European Journal of Wood and Wood Products* 71(4), 525-527. DOI: 10.1007/s00107-013-0696-1

Matsumoto, N., and Nairn, J. A. (2009). "The fracture toughness of medium density fiberboard (MDF) including the effects of fiber bridging and crack-plane interference," *Engineering Fracture Mechanics* 76(18), 2748-2757. DOI: 10.1016/j.engfracmech.2009.04.007

Oliveira, J. M. Q., de Moura, M. F. S. F., Silva, M. A. L., and Morais, J. J. L. (2007). "Numerical analysis of the MMB test for mixed-mode I/II wood fracture," *Composites Science and Technology* 67(9), 1764-1771. DOI: 10.1016/j.compscitech.2006.11.007

Omrani, P., Mansouri, H. R., and Pizzi, A. (2009). "Influence of wood grain direction on linear welding," *Journal of Adhesion Science and Technology* 23(16), 2047-2055. DOI: 10.1163/016942409X12526743387845

Omrani, P., Mansouri, H. R., Pizzi, A., and Masson, E. (2010). "Influence of grain direction and pre-heating on linear wood welding," *European Journal of Wood and Wood Products* 68(1), 113-114. DOI: 10.1007/s00107-009-0349-6

Pavkovic, K., Rajcic, V., and Cizmar, D. (2014). "Parametric analysis of large diameter mechanical fastener in reinforced glulam," *Tehnicki Vjesnik-Technical Gazette* 21(4), 843-852.

Pena, M. I. P., Deutschle, A. L., Saake, B., Pizzi, A., and Pichelin, F. (2016). "Study of the solubility and composition of welded wood material at progressive welding times," *European Journal of Wood and Wood Products* 74(2), 191-201. DOI: 10.1007/s00107-015-0991-0

Pizzi, A. (2006). "Recent developments in eco-efficient bio-based adhesives for wood bonding: Opportunities and issues," *Journal of Adhesion Science and Technology* 20(8), 829-846. DOI: 10.1163/156856106777638635

Pizzi, A., Properzi, M., Leban, J.-M., Zanetti, M., and Pichelin, F. (2003). "Mechanically-induced wood welding," *Maderas. Ciencia y Tecnología* 5(2), 101-106. DOI: 10.4067/S0718-221X2003000200001

Saavedra Flores, E. I., Saavedra, K., Hinojosa, J., Chandra, Y., and Das, R. (2016). "Multi-scale modelling of rolling shear failure in cross-laminated timber structures by homogenisation and cohesive zone models," *International Journal of Solids and Structures* 81, 219-232. DOI: 10.1016/j.ijsolstr.2015.11.027

Silva, M. A. L., Morais, J. J. L., de Moura, M. F. S. F., and Lousada, J. L. (2007). "Mode II wood fracture characterization using the ELS test," *Engineering Fracture Mechanics* 74(14), 2133-2147. DOI: 10.1016/j.engfracmech.2006.10.012

Stamm, B., Natterer, J., and Navi, P. (2005a). "Joining of wood layers by friction welding," *Journal of Adhesion Science and Technology* 19(13-14), 1129-1139. DOI:

10.1163/156856105774429046
Stamm, B., Natterer, J., and Navi, P. (2005b). "Joining wood by friction welding," *Holz Als Roh-Und Werkstoff* 63(5), 313-320. DOI: 10.1007/s00107-005-0007-6
Sun, Q., Yi, X., Lu, X., Ju, Z., and Zhang, H. (2019). "Enhancement of gluability of poplar with linear vibration friction welding," *Journal of Forestry Engineering* 4(3), 32-37.
Tran, V.-D., Oudjene, M., and Meausoone, P.-J. (2014a). "FE analysis and geometrical optimization of timber beech finger-joint under bending test," *International Journal of Adhesion and Adhesives* 52, 40-47. DOI: 10.1016/j.ijadhadh.2014.03.007
Tran, V. D., Oudjene, M., and Meausoone, P. J. (2014b). "FE analysis and geometrical optimization of timber beech finger-joint under bending test," *International Journal of Adhesion and Adhesives* 52, 40-47. DOI: 10.1016/j.ijadhadh.2014.03.007
Vallee, T., Hahn, B., and Weinand, Y. (2017). "Shear loaded friction-welded crosswise arranged timber boards," *International Journal of Adhesion and Adhesives* 72, 109-116. DOI: 10.1016/j.ijadhadh.2016.10.016
Vallee, T., Weinand, Y., Hahn, B., and Stamm, B. (2011). "Numerical modelling and strength prediction of welded double lap joints made of timber," in: *11th International Conference on the Mechanical Behavior of Materials (ICM)*, 2011, Como, Italy, pp. 1309-1314. DOI: 10.1016/j.proeng.2011.04.218
Vaziri, M., Abrahamsson, L., Hagman, O., and Sandberg, D. (2020). "Welding of wood in the presence of wollastonite," *BioResources* 15(1), 1617-1628. DOI: 10.15376/biores.15.1.1617-1628
Vaziri, M., Lindgren, O., and Pizzi, A. (2012). "Optimization of tensile-shear strength for linear welded Scots pine," *Journal of Adhesion Science and Technology* 26(1-3), 109-119. DOI: 10.1163/016942411X569327
Xavier, J., Oliveira, M., Monteiro, P., Morais, J. J. L., and de Moura, M. F. S. F. (2014a). "Direct evaluation of cohesive law in mode I of *Pinus pinaster* by digital image correlation," *Experimental Mechanics* 54(5), 829-840. DOI: 10.1007/s11340-013-9838-y
Xavier, J., Oliveira, M., Morais, J. J. L., and de Moura, M. F. S. F. (2014b). "Determining mode II cohesive law of Pinus pinaster by combining the end-notched flexure test with digital image correlation," *Construction and Building Materials* 71, 109-115. DOI: 10.1016/j.conbuildmat.2014.08.021
Zhang, H., Pizzi, A., Lu, X., and Zhou, X. (2014). "Optimization of tensile shear strength of linear mechanically welded outer-to-inner flattened moso bamboo (*Phyllostachys pubescens*)," *BioResources* 9(2), 2500-2508. DOI: 10.15376/biores.9.2.2500-2508
Zhang, H., Zhou, X., Lu, X., Wang, Z., and Zhu, N. (2015). "Study on the bonding strength of the linear-vibration mechanical welded Moso bamboo," *Journal of Nanjing Forestry University. Natural Sciences Edition* 39(5), 135-138.
Zhang, J., He, M.-J., and Li, Z. (2018). "Numerical analysis on tensile performance of bolted glulam joints with initial local cracks," *Journal of Wood Science* 64(4), 364-376. DOI: 10.1007/s10086-018-1709-9
Zhu, X., Yi, S., Gao, Y., Zhang, J., Ni, C., and Luo, X. (2017). "Influence of welded depth and CuCl2 pretreated dowels on wood dowel welding," *Journal of Wood Science* 63(5), 445-454. DOI: 10.1007/s10086-017-1644-1

Zigon, J., Pizzi, A., Zhang, H., Sega, B., Cop, M., and Sernek, M. (2015). "The influence of heat and chemical treatments of beech wood on the shear strength of welded and UF bonded specimens," *European Journal of Wood and Wood Products* 73(5), 685-687. DOI: 10.1007/s00107-015-0930-0

Zor, M., and Can, A. (2021). "Shear strength in friction welded joint of poplar wood impregnated with copper-based wood preservative," *Maderas-Ciencia y Tecnologia* 23, 8. DOI: 10.4067/S0718-221X2021000100409

Article submitted: February 22, 2024; Peer review completed: October 5, 2025; Revised version received and accepted: October 6, 2025; Published: October 27, 2025.
DOI: 10.15376/biores.20.4.10665-10684